IEEE TRANSACTIONS ON ANTENNAS AND PROPAGATION

The following publication J. -Y. Deng, Y. Zhang and W. Lin, "Compact Multibeam Antenna Array Facilitated by Miniaturized Slow Wave Substrate Integrated Waveguide Butler Matrix," in IEEE Transactions on Antennas and Propagation, vol. 72, no. 12, pp. 9564-9569, Dec. 2024 is available at https://doi.org/10.1109/TAP.2024.3463203.

Compact Multibeam Antenna Array Facilitated by Miniaturized Slow Wave Substrate Integrated Waveguide Butler Matrix

Jing-Ya Deng, Member, IEEE, Yin Zhang and Wei Lin, Senior Member, IEEE

Abstract—This paper presents a compact multibeam antenna array facilitated by a 4 × 4 Butler matrix with substantially miniaturized dimensions based on slow wave substrate integrated waveguide (SW-SIW). It is well known that conventional Butler matrix is bulky as the beamformer that occupies most area of the multibeam array. In this work, the miniaturization of the Butler matrix is realized by loading slow wave (SW) structures in the form of loaded patches and blind via-holes into substrate integrated waveguide (SIW). In this manner, the effective permittivity and permeability of the SIW are increased. Consequently, both the guided wavelength and the cut-off frequency of the SIW are largely reduced. This SW-SIW technology enables the designs of miniaturized couplers, crossovers, and phase shifters with substantially reduced longitudinal and lateral dimensions. With these miniaturized components, a Butler matrix with excellent performance is developed, which is 75.5% smaller compared with conventional SIW-based Butler matrix. The miniaturized 4×4 Butler matrix is then employed to design a compact four-beam slot antenna array. The measured results agree reasonably well with the simulations, demonstrating the feasibility of the miniaturized SW-SIW Butler matrix in designing compact multibeam antenna array.

Index Terms-Butler matrix, miniaturization, multibeam antenna array, SIW, substrate integrated waveguide, slow wave.

I. INTRODUCTION

As typical passive beamforming networks, Butler matrices have been extensively studied and adopted for multibeam antennas [1-2]. The Butler matrix was initially invented by J. Butler in [3]. The early implementations of Butler matrices utilized metallic waveguides [4], which suffered from bulky size and heavy weight due to their nonplanar structures. Subsequently, Butler matrices based on microstrip lines [5] and coplanar waveguides (CPW) [6] were developed, offering advantages such as compactness, lightweight, cost-effectiveness, and high integration levels. However, the nonenclosed natures of microstrip and CPW configurations resulted in significant radiation loss and mutual coupling between neighboring components [7]-[9].

The substrate integrated waveguide (SIW) was introduced in [10] that features the advantages such as low loss, cost-effectiveness, lightweight, and high integration levels. The first realization of a SIW Butler matrix was presented in [11], followed by the development and investigation of planar SIW Butler matrices in [12]-[14]. In spite of the aforementioned merits, SIW-based Butler matrix still suffers from bulky size as many couplers, crossovers, and phase shifters are required that may occupy much larger area than antenna radiators.

Some miniaturized SIW Butler matrices have been proposed in the literatures. A stacked SIW Butler matrix was developed in [15] with

This work was supported in part by National Natural Science Foundation of China for Outstanding Young Scholars under Grant 62022064, and in part by the Research Grants Council of Hong Kong, SAR, China, under Project PolyU 25213623 and AoE/E-101/23-N. (Corresponding author: Wei Lin).

Jing-Ya Deng and Yin Zhang are with School of Physics, Xidian University, Xi'an 710071, China. (E-mail: jydeng@xidian.edu.cn)

Wei Lin is with the Photonics Research Institute, Department of Electrical and Electronic Engineering, The Hong Kong Polytechnic University, Hong Kong SAR, China (e-mail: w.lin@polyu.edu.hk).

reduced the dimensions, but the multilayer structure increases the fabrication complexity. In [16], by introducing the defected ground structure in the form of interdigital slots, the longitudinal size of SIW Butler matrix was reduced by 32%.

To realize miniaturization for planar circuits, slow wave SIW (SW-SIW) was invented in [17] and extensively investigated [18]-[20]. Slow wave structures used in this paper can reduce the guided wavelength of the electromagnetic wave and decrease the cutoff frequency of the SIW [20], [21].

This paper has successfully addressed a long-lasting challenge for the miniaturization of multi-beam antenna based on Butler matrix and SIW. For instance, SW-based crossovers and phase shifters are reported at the first time that are effectively integrated with other components, i.e., couplers, transitions and SIW transmission lines, in a 4×4 multi-beam antenna array. Excellent transmission performance is achieved. Noticeably, the new design is more than 75.5% smaller compared with the conventional SIW-based Butler matrix. Then a ultracompact multibeam antenna array excited by the miniaturized SW-SIW Butler matrix is designed in Ku band that has been widely adopted for satellite applications. The prototype was fabricated and the measured results are in reasonable agreement with the simulations, confirming the developed miniaturized SW-SIW Butler matrix is an excellent beamformer for compact antenna array systems.

II. DESIGN OF THE SW-SIW BASED MINIATURIZED BUTLER MATRIX

The configuration of the proposed miniaturized SW-SIW Butler matrix is illustrated in Fig. 1. It consists of four 3-dB quadrature couplers, two crossovers, two 45° phase shifters, and two 0° phase shifters, all based on SW-SIWs. The topology is implemented using two Rogers 5880 substrates with a dielectric constant of 2.2 and a loss tangent of 0.0009.

The miniaturized Butler matrix proposed in this study utilizes the SW-SIW [20] that is loaded with metallized blind via-holes and shorted patches. Inside the lower substrate, metallized via-holes are loaded. On the top surface of the lower substrate, metal patches are printed and electrically connected to the blind via holes. These metallized blind via-holes and patches are periodically distributed along the longitudinal direction. The mechanism and design guideline of this kind of SW-SIW have been clearly demonstrated in [20], which are not provided here to avoid unnecessary repetition.

A. Miniaturized 3-dB Coupler Based on SW-SIW

Couplers are essential components in Butler matrices. Fig. 2 shows the configuration of the miniaturized 3-dB quadrature coupler based on SW-SIW that consists of two SW-SIW transmission lines and a coupling slot. In the lower substrate of the coupler, slow wave structures are introduced by loading three rows of metallized blind via-holes and shorted patches. As shown in Fig. 2 (b), Port 1, 2, 3, 4 are input, through, coupled and isolated ports respectively.

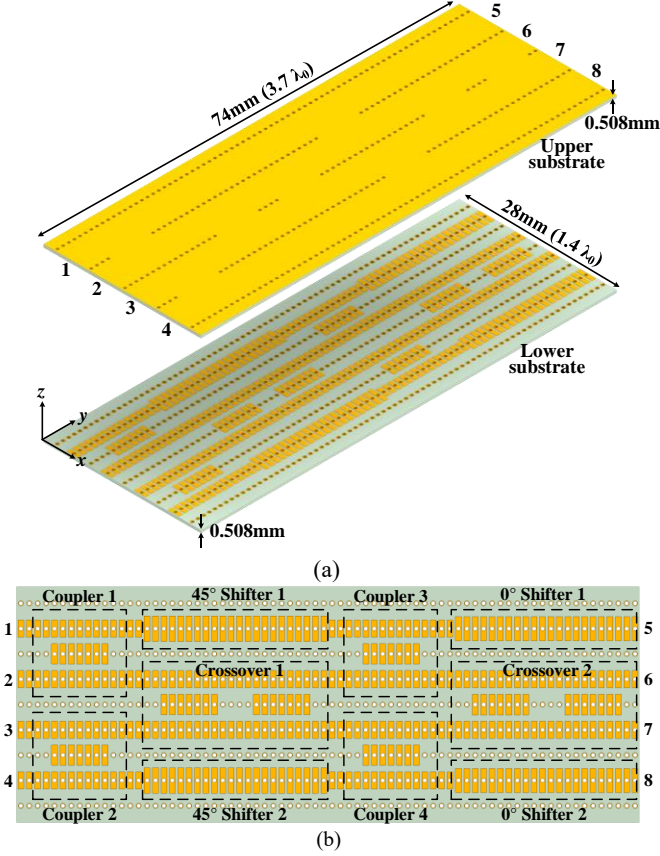


Fig. 1. Configuration of the SW-SIW Butler matrix. (a) Exploded 3-D view, (b) Top view of lower substrate.

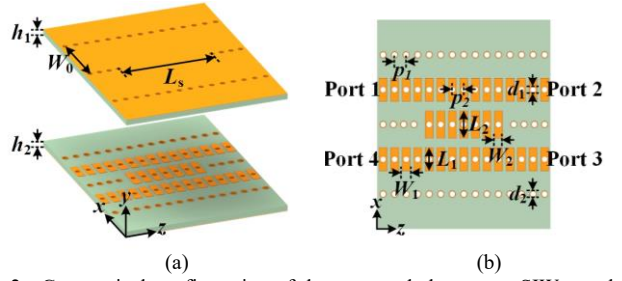


Fig. 2. Geometrical configuration of the proposed slow wave SIW coupler. (a) Exploded 3-D view. (b) Top view of lower substrate. $(h_1=h_2=0.508, L_s=7.86, L_1=2, L_2=2.35, W_0=6, W_1=W_2=0.7, p_1=p_2=1, d_1=d_2=0.5\text{mm})$

The SW-SIW width W_0 is set as 6 mm, ensuring the cutoff frequency is lower than the operation frequency of the coupler. Initially, two SW-SIW transmission lines are placed side by side and a coupling slot is created by removing several metallized via-holes of the shared wall. The propagation constants of TE₁₀ and TE₂₀ modes in the coupling region of the original SW-SIW coupler are shown in Fig. 3, the propagation constants of TE₁₀ and TE₂₀ modes are β_{10} =553.2 rad/m and β_{20} =403.6 rad/m respectively at 15 GHz. The coupling slot length $L_{\rm s}$ of the original SW-SIW coupler is calculated as 11.14 mm according to the design guideline of 3-dB short-slot couplers [22]:

$$\left(\beta_1 - \beta_2\right) L_s = \frac{\pi}{2} \tag{1}$$

where β_1 and β_2 are the propagation constants of the TE₁₀ and TE₂₀ modes in the coupling region respectively, L_s is the length of coupling slot.

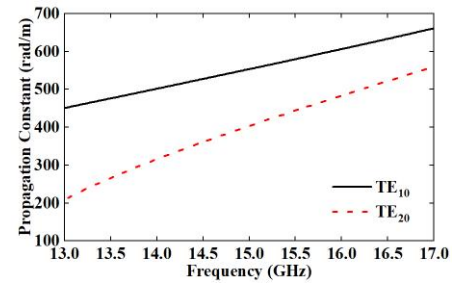


Fig. 3. Propagation constants of TE_{10} and TE_{20} modes in the coupling region.

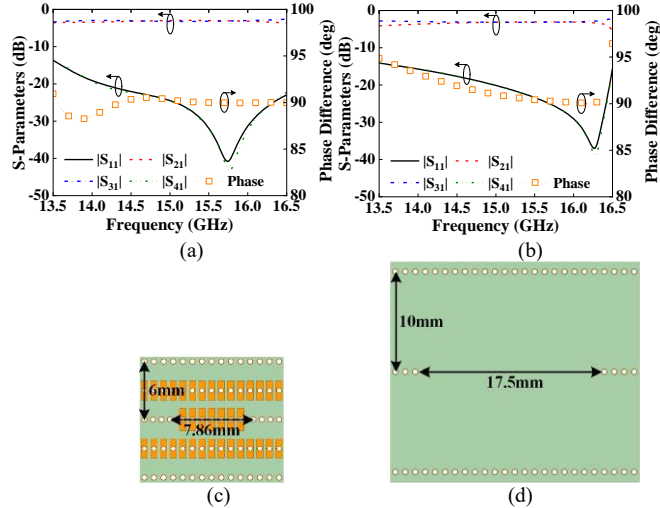


Fig. 4. Simulated S-parameters of the (a) SW-SIW coupler. (b) Simulated S-parameters of the normal SIW coupler. (c) Dimensions of SW-SIW coupler, (d) Dimensions of normal SIW coupler.

As indicated by (1), the coupling slot length is inverse-proportionally correlated to the difference between propagation constants of the TE₁₀ and TE₂₀ modes. The maximum electric field of the TE₁₀ mode occurs around the coupling slot, where the electric field of the TE₂₀ mode is at its minimum. By adjusting the size of the slow wave structures in the coupling slot, the propagation constant β_1 of the TE₁₀ mode can be modified without affecting the TE₂₀ mode. In this study, increasing the length L_2 of the shorted patches at the coupling slot enhances the capacitance between the shorted patches and the top ground plane, thus intensifying the slow wave effect in the coupling slot. Consequently, the propagation constant of the TE₁₀ mode is increased, resulting in an enlarged difference in propagation constants between the TE₁₀ and TE₂₀ modes. As a result, the length of the coupling slot L_s is reduced from 11.4 mm to 7.86 mm, further miniaturizing the longitudinal dimension of the coupler.

The simulated S-parameters and the phase difference between through and coupled ports of the SW-SIW coupler are shown in Fig. 4 (a). The amplitude imbalance between the through and coupled ports is lower than 1 dB from 13.5 to 16.5 GHz. The phase difference between through and coupled ports is 90°±5°. To show the miniaturization effect of the SW-SIW coupler, the dimensions of the SW-SIW coupler are compared with conventional SIW coupler in Fig. 4 (c) and (d). The dimensions of the SW-SIW coupler are noticeably reduced by 73% from 350 mm² to 94.32 mm². As shown in Fig. 4 (b), the S-parameters of the SW-SIW coupler remains desired despite its reduced size.

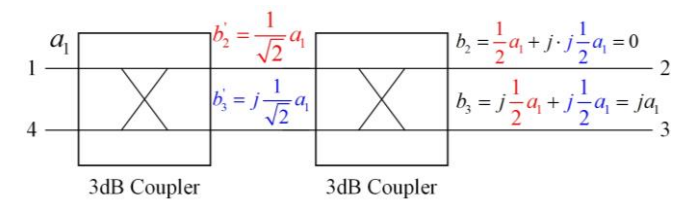


Fig. 5. Block diagram of crossover cascaded by two identical 3-dB quadrature couplers.

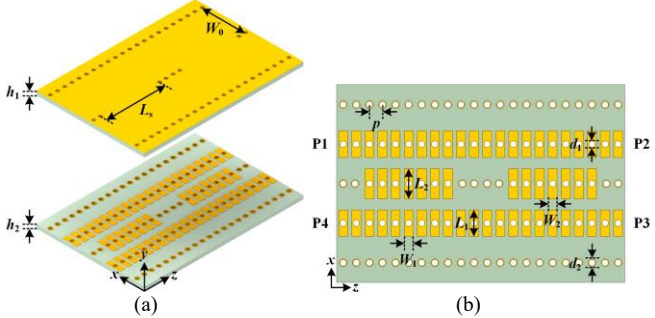


Fig. 6. Configuration of the SW-SIW crossover. (a) Exploded 3-D view. (b) Top view of lower substrate. (h_1 = h_2 =0.508, L_s =7.86, L_1 =2, L_2 =2.35, W_1 = W_2 =0.7, p=1, d_1 = d_2 =0.5mm)



Fig. 7. Electric field distribution on the H-plane of SW-SIW crossover.

B Miniaturized Crossover Based on SW-SIW

Crossovers, whose block diagram is shown in Fig. 5, can be realized by cascading two identical 3-dB quadrature couplers. To clearly illustrate the operating principle, we consider the excitation of Port 1 with a signal phase of 0°, and thus signals with phase 0° and -90° will be generated at b_2 ' and b_3 ', respectively. For the signal at b_2 ', signals with phases of 0° and -90° are generated at Port 2 and Port 3, respectively. Similarly, originating from the signal at b_3 , signals with phases of -180° and -90° are generated at Port 2 and Port 3, respectively. As a result, the two signals at Port 2 are out of phase, while the signals at Port 3 are in phase. This implies that there is no signal at Port 2, and the electromagnetic wave can directly propagate from Port 1 to Port 3. Similarly, the wave can directly propagate from Port 4 to Port 2 due to the symmetry of the crossover. The SW-SIW crossover configuration is depicted in Fig. 6, consisting of two cascaded SW-SIW couplers. Each coupler's dimensions are the same as those mentioned in Section II A.

The electric field distribution in the SW-SIW crossover when Port 1 is excited is shown in Fig. 7. The electromagnetic wave propagates diagonally across to Port 3, while very little energy is transmitted to Port 2. This behavior ensures the successful achievement of the crossover function. Similarly, if Port 4 is excited, the electromagnetic wave will propagate diagonally across to Port 2, while very little energy is transmitted to Port 3.

The simulated S-parameters of the SW-SIW crossover are shown in Fig. 8 (a). The insertion loss remains below 0.18 dB across the frequency range from 13.5 to 16.5 GHz. To demonstrate the miniaturization effect of the SW-SIW crossover, a comparison of the dimensions between the SW-SIW crossover and a conventional SIW crossover is presented in Fig. 8 (c) and (d). It can be observed that

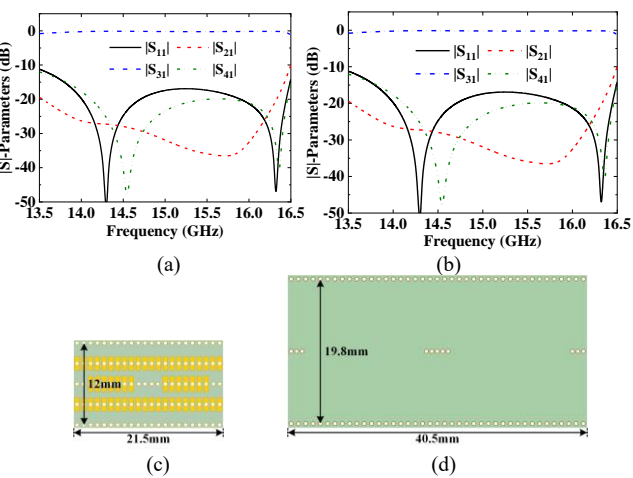


Fig. 8. (a) S-parameters of SW-SIW crossover. (b) S-parameters of normal SIW crossover, (c) Dimensions of SW-SIW crossover, (d) Dimensions of normal SIW crossover.

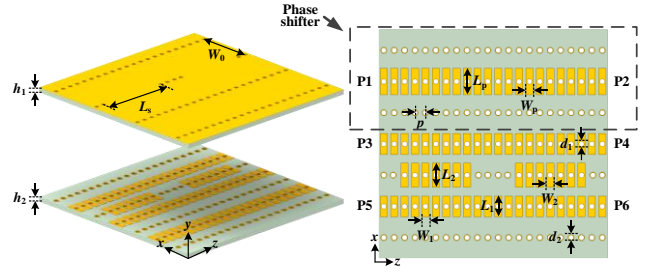


Fig. 9. Configuration of the SW-SIW phase shifter. (a) Exploded 3-D view. (b) Top view of lower substrate. (h_1 = h_2 =0.508, L_s =7.86, L_1 =2, L_2 =2.35, W_1 = W_2 =0.7, p=1, d_1 = d_2 =0.5mm)

the area is reduced by 67.8%, from 801.9 mm² (40.5mm×19.8mm) to 258 mm² (21.5mm×12mm). Despite this substantial reduction in size, the S-parameter performances of the miniaturized SW-SIW crossover remain comparable with the conventional SIW crossover shown in Fig. 8 (b).

C. Miniaturized Phase Shifter Based on SW-SIW

The phase shifter's configuration is illustrated in Fig. 9. Slow wave structures (SWS) that increases the propagation constant of the SIW have significant impacts on wave's phase. Therefore, in the proposed Butler matrix, the desired phase shifters are realized by simply adjusting the dimensions of the SWS. By increasing the length of the patch $L_{\rm P}$, the propagation constant can be increased [20]. It is feasible to implement 45° and 0° phase shifters within the SW-SIW Butler matrix by properly controlling the propagation constant of the SW-SIW. This control is facilitated by adjusting the length of the short patches.

By adjusting the length (L_p) of the shorted patches in the SW- SIW between Port 1 and Port 2, the 45° and 0° phase shifters are successfully realized. It is noted that the patch length (L_p) is set at 2.9 mm for the 0° phase shifter and 3.1mm for the 45° phase shifter. The S-parameters and phase characteristics of the proposed phase shifters are presented in Fig. 10 (a) and (b), respectively. For the 0° phase shifter, the phase difference between Port 2 and Port 6 is 0°±15° within 14 to 16 GHz. The reflection coefficient remains lower than -10 dB, and the insertion loss is better than 0.12 dB. Similarly, for the 45° phase shifter, the phase difference between Port 2 and Port 6 is 45°±15° within the 14 to 16 GHz frequency range. The reflection coefficient remains lower than -10 dB, and the insertion loss is better than 0.13 dB in the operating band.

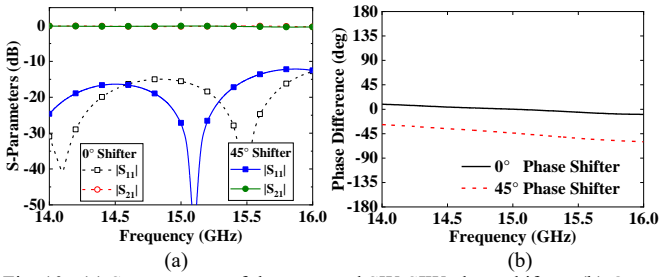


Fig. 10. (a) S-parameters of the proposed SW-SIW phase shifters, (b) Output phases of the proposed SW-SIW phase shifters.

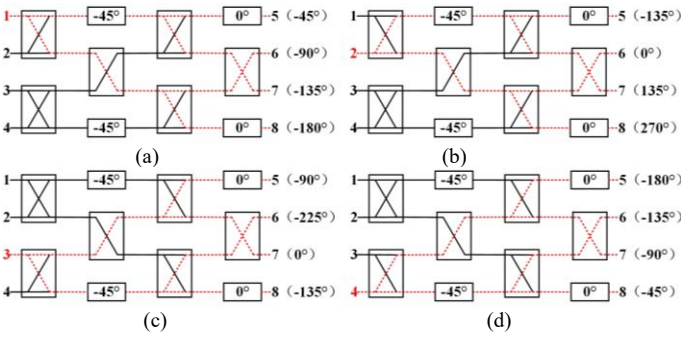


Fig. 11. Signal-flow diagram of SW-SIW Butler matrix. Port 1, 2, 3, and 4 are excited for (a), (b), (c), and (d) respectively.

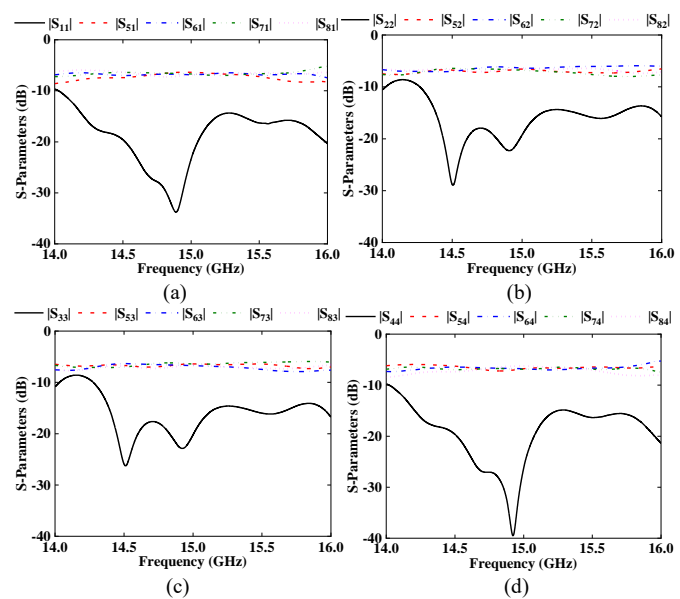


Fig. 12. S-parameters of the proposed SW-SIW Buter matrix. (a) Port 1 is fed. (b) Port 2 is fed. (c) Port 3 is fed. (d) Port 4 is fed.

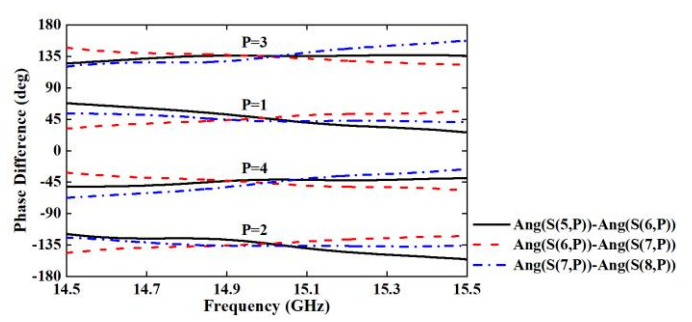


Fig. 13. Phase differences between output ports of the SW-SIW Buter matrix.

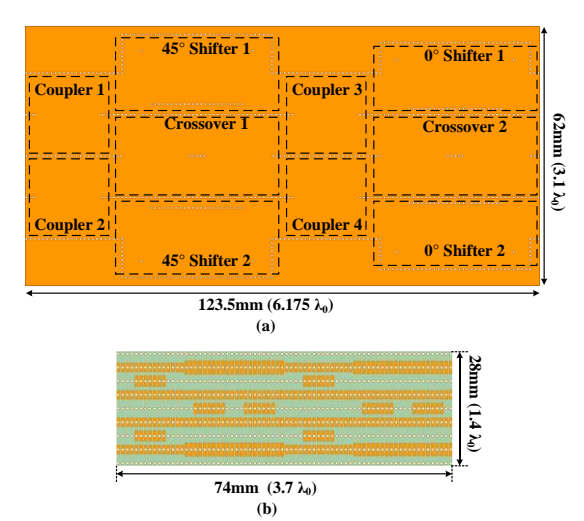


Fig. 14. Comparison of the overall sizes of the Butler matrices. (a) Normal SIW Butler matrix. (b) SW-SIW Butler matrix.

D Miniaturized Butler Matrix Based on SW-SIW

The SW-SIW Butler matrix is realized by cascading the above SW-SIW components, including four SW-SIW 3-dB quadrature couplers, two SW-SIW crossovers, two SW-SIW 45° phase shifters and two SW-SIW 0° shifters. The configuration of the proposed SW-SIW miniaturized Butler matrix is shown in Fig. 1 and its overall size is $74\text{mm} \times 28\text{mm}$ (3.7 $\lambda_0 \times 1.4 \lambda_0$ at center frequency 15 GHz).

The signal-flow diagram of SW-SIW Butler matrix with different input port excited is shown in Fig. 11. The simulated S-parameters of the miniaturized SW-SIW Butler matrix are shown in Fig. 12. For each input port, the transmission coefficients (S_{5p} , S_{6p} , S_{7p} , S_{8p} , p = 1, 2, 3, 4) are around -6.6 ± 1 dB from 14.5 to 15.5 GHz. The insertion losses are around 0.6 dB. The Butler matrix achieves equal power division among the output ports 5-8 regardless of which input port (1-4) is excited. This demonstrates that the matrix effectively distributes the input power evenly across the output ports.

Fig. 13 illustrates the simulated phase differences between two adjacent output ports under different excitations of input ports 1, 2, 3, and 4. The phase differences between two adjacent output ports are $45^{\circ}\pm15^{\circ}$, $-135^{\circ}\pm15^{\circ}$, $135^{\circ}\pm15^{\circ}$ and $-45^{\circ}\pm15^{\circ}$ from 14.6 to 15.4 GHz when the input port 1, 2, 3 and 4 is excited, respectively.

To demonstrate the miniaturization achieved by the SW-SIW Butler matrix, a conventional SIW-based Butler matrix is designed for comparison in terms of the dimensions and the transmission performances. The configuration of the conventional SIW-based Butler matrix is shown in Fig. 14 (a). The S-parameters and phase differences between two adjacent output ports of the normal SIWbased Butler matrix are shown in Fig. 15 and 16, respectively. The transmission performances of the proposed SW-SIW Butler matrix are comparable to the normal SIW Butler matrix. As compared in Fig. 14, the size of the SW-SIW Butler matrix working at center frequency 15 GHz is 74mm \times 28mm (3.7 $\lambda_0 \times$ 1.4 λ_0), while the normal SIW-based Butler matrix's size working at same center frequency is 123.5mm \times 62mm (6.175 $\lambda_0 \times 3.1 \lambda_0$). The area of the Butler matrix is reduced by 75.5%. Comparing Figs. 13 and 16 reveals that the phase differences between the outputs of the SW-SIW Butler matrix are greater than those of the conventional SIW Butler matrix. This is due to the dispersion effects of the slow-wave structures in the SW-SIW. As a result, the bandwidth of the SW-SIW Butler matrix is somewhat reduced.

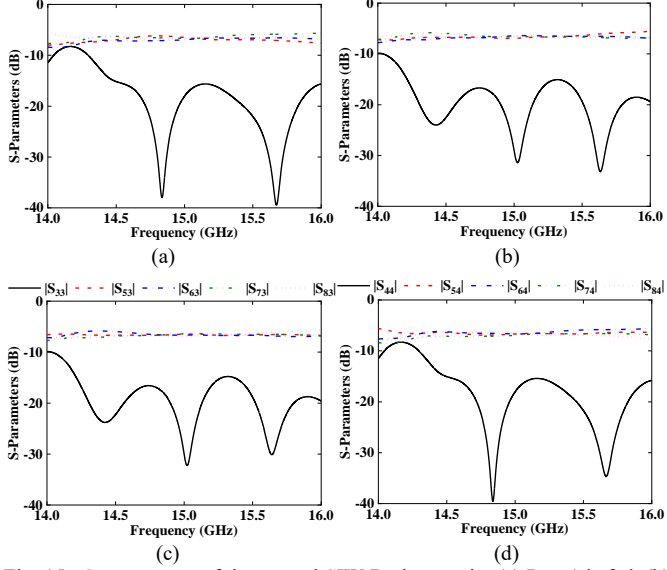


Fig. 15. S-parameters of the normal SIW Butler matrix. (a) Port 1 is fed. (b) Port 2 is fed. (c) Port 3 is fed. (d) Port 4 is fed.

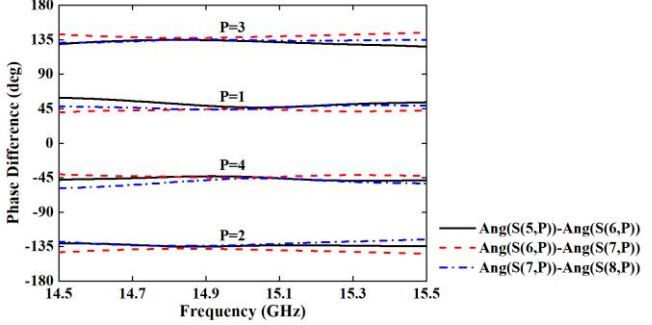


Fig. 16. Phase difference between output ports of the normal SIW Butler matrix.

TABLE I Comparisons of Different Butler Matrices

Ref.	Freq. (GHz)	Trans. Line	Type	Dimensions (L×W×H) (λ_0^3)
13	60	SIW	4×4	$5.42 \times 3.56 \times 0.0254 \approx 0.49$
14	30	SIW	4×4	$5.56 \times 2.74 \times 0.0508 \approx 0.774$
15	30	C-SIW	4×4	$5.54 \times 1.24 \times 0.1016 \approx 0.698$
16(1)	30	SIW	4×4	$3.78 \times 2.74 \times 0.0508 \approx 0.526$
16(2)	30	SIW	4×4	$2.96 \times 0.76 \times 0.2032 \approx 0.457$
16(3)	30	FC-SIW	4×4	3.84×1.24×0.1016≈0.484
This Work	15	SW-SIW	4×4	3.7×1.4×0.0508≈0.263

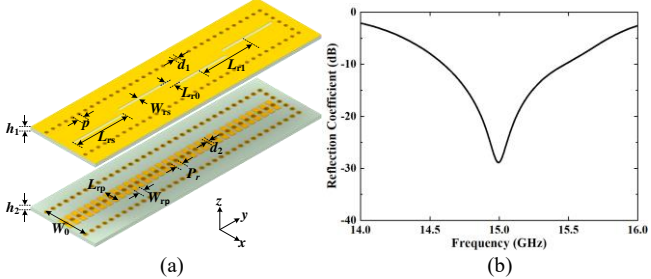


Fig. 17. (a) Configuration, and (b) reflection coefficient of the four element SW-SIW slot array. (h_1 = h_2 =0.508, W_0 =6, Lrs=7.4, Wrp=0.7, Lrp=1, Wrs=0.2, Lr_0 =0.4, Lr_1 =7.7, L_s =7.86, p= p_r =1, d_1 = d_2 =0.5mm)

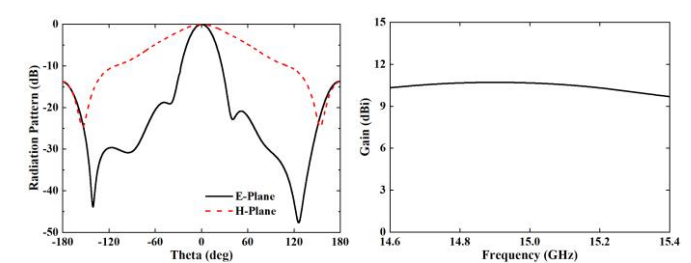


Fig. 18. (a) Normalized pattern and (b) gains of the SW-SIW slot array

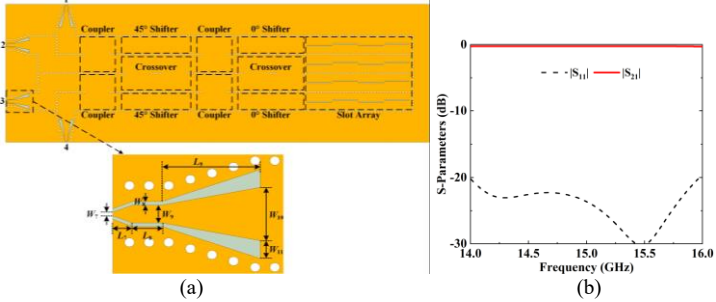


Fig. 19. (a) Configuration of the SW-SIW Butler matrix multibeam antenna with transitions. (L_7 =1, L_8 =1.5, L_9 =5, W_7 =0.2, W_8 =0.1, W_9 =1, W_{10} =3, W_{11} =1mm) (b) S-Parameters of the transition

Table I presents a comparison between the proposed SW-SIW Butler matrix and existing 4×4 SIW Butler matrices in the literatures, highlighting the miniaturization effect achieved. The result illustrates that the SW-SIW Butler matrix design has been successfully miniaturized with the smallest electrical dimensions, showcasing the advantage of SW-SIW in beamforming network design.

III. DESIGN OF THE COMPACT MULTIBEAM ANTENNA ARRAY BASED ON THE MINIATURIZED SW-SIW BUTLER MATRIX

To validate the feasibility of the proposed miniaturized SW-SIW Butler matrix, a compact SW-SIW multibeam antenna array system is designed by integrating SW-SIW slot arrays with the miniaturized SW-SIW Butler matrix.

A four element SW-SIW slot array shown in Fig. 17 (a) is designed as the radiating parts of a 4×4 multibeam antenna array system by two layers of stacked substrates. Slow wave structures in the form of metallized blind via-holes and shorted patches are loaded in the lower substrate. Four radiating slots are etched on the top plane of upper substrate. The lengths of the slots and the distances between adjacent slots are approximately set to half of the guided wavelength. It should be noted that the slow wave structures loaded in the lower substrate of the slot arrays are necessary in this design to decrease the cutoff frequency of the SIW. Otherwise, none of the electromagnetic wave can propagate into the slot array, because the cutoff frequency of a 6mm-wide normal SIW implemented by Rogers 5880 substrate is higher than the working frequency of the SW-SIW Butler matrix. The reflection coefficient of the four element SW-SIW slot array is better than -10 dB from 14.6 to 15.4 GHz as shown in Fig. 17(b). The normalized radiation patterns at the center frequency 15GHz are shown in Fig. 18 (a). The gain of the four element SW-SIW slot array is higher than 9.8 dBi in the operation band as shown in Fig. 18 (b).

By cascading four slot array at the output ports of the SW-SIW Butler matrix, a 4×4 multibeam antenna array system can be formed. The transitions from grounded coplanar waveguide (GCPW) to SW-SIW are adopted at input ports as shown in Fig. 19 (a), whose S-parameters are given in Fig. 19 (b).

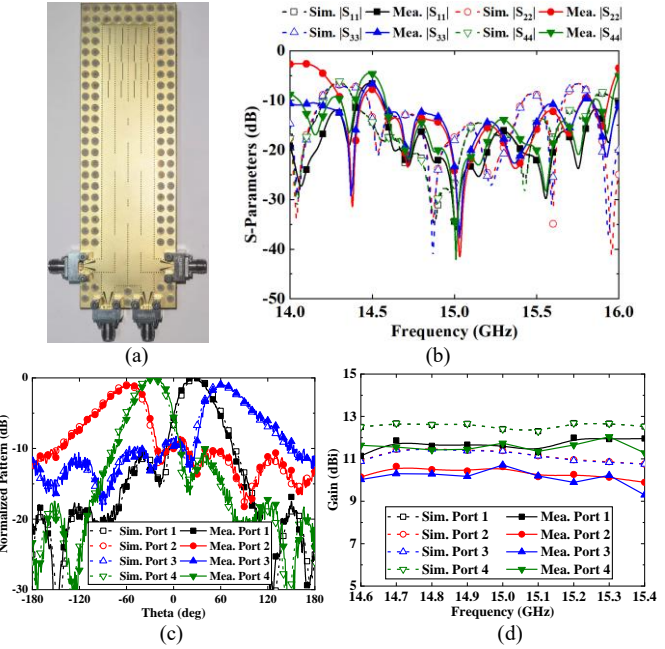


Fig. 20. (a) Photo, (b) S-parameters, (c) normalized patterns (d) gains of the proposed SW-SIW multibeam antenna

A prototype of the multibeam antenna array based on the SW-SIW Butler matrix is manufactured and measured as shown in Fig. 20 (a). The simulated and measured S-parameters of the SW-SIW multibeam antenna are given in Fig. 20 (b). The simulated reflection coefficients are lower than -10 dB from 14.5-15.4 GHz, while the measured ones are better than -10 dB from 14.6-15.6 GHz. Fig. 20 (c) illustrates the simulated and measured radiation patterns of the SW-SIW multibeam antenna array when different ports are excited. At the center frequency 15 GHz, the beam directions are 32°, -59°, 59°, and -32°, corresponding to the feeding ports 1, 2, 3, and 4. The simulated and measured realized gains of the SW-SIW multibeam antenna system with different input ports excited are presented in Fig. 20 (d). When Port 1 or Port 4 is excited, the simulated gain ranges from 12.2 to 12.7 dBi, while the measured gain ranges from 11.1 to 12.1 dBi. When Port 2 or Port 3 is excited, the simulated gain ranges from 10.8 to 11.5 dBi, and the measured gain ranges from 9.2 to 10.8 dBi. The difference values between simulated and measured gains, deducting the connector loss, are not greater than 0.46 dB. These experimental results demonstrate the effectiveness of the miniaturized SW-SIW Butler matrix in achieving compact SW-SIW multibeam antenna array with reasonable gain values.

IV. CONCLUSION

This paper introduced a compact multibeam antenna array facilitated by miniaturized SW-SIW Butler matrix. The antenna utilizes a 4×4 Butler matrix with greatly reduced dimensions that is realized by adopting the slow wave substrate integrated waveguide (SW-SIW) technology. The SW-SIW Butler matrix realize a 75.5% overall size reduction compared with a conventional SIW-based Butler matrix. The measured results align reasonably well with the simulations, indicating that the compact multibeam antenna based on the miniaturized Butler matrix offers a competitive solution for space-constrained scenarios of multibeam applications. The proposed compact multibeam antenna array and miniaturized SW-SIW Butler matrix can be scaled to higher frequencies, i.e. the millimeter-wave band. This scaling will require more precise manufacturing processes to accurately fabricate the slow-wave structures.

REFERENCES

- W. Hong et al., "Multibeam Antenna Technologies for 5G Wireless Communications," *IEEE Trans. Antennas Propagat.*, vol. 65, no. 12, pp. 6231-6249, Dec. 2017.
- [2] Y. J. Guo, M. Ansari and N. J. G. Fonseca, "Circuit Type Multiple Beamforming Networks for Antenna Arrays in 5G and 6G Terrestrial and Non-Terrestrial Networks," *IEEE Journal of Microwaves*, vol. 1, no. 3, pp. 704-722, July 2021.
- [3] J. Butler and R. Lowe, "Beamforming matrix simplifies design of electronically scanned antennas," *Electron. Des.*, vol. 9, pp. 170–173, Apr. 1961.
- [4] R. S. Davis and H. E. Schrank, "Application of the Butler Matrix to High-Power Multichannel Switching," G-MTT Symposium Digest, 1965, pp. 133-138.
- [5] J. R. Wallington, "Analysis, Design and Performance of a Microstrip Butler Matrix," 1973 3rd European Microwave Conference, 1973, pp. 1-4.
- [6] M. Nedil, T. A. Denidni and L. Talbi, "Novel butler matrix using CPW multilayer technology," *IEEE Trans. Microw. Theory Techn.*, vol. 54, no. 1, pp. 499-507, Jan. 2006.
- [7] W. P. Harokopus and L. P. B. Katehi, "Electromagnetic coupling and radiation loss considerations in microstrip (M)MIC design," *IEEE Trans. Microw. Theory Techn.*, vol. 39, no. 3, pp. 413-421, Mar. 1991.
- [8] W. P. Harokopus and P. B. Katehi, "Radiation loss from open coplanar waveguide discontinuities," *IEEE MTT-S Int. Microw. Symp. Dig.*, Boston, MA, USA, 1991, pp. 743-746.
- [9] J. Bernal, F. Mesa and D. R. Jackson, "Crosstalk in Coupled Microstrip Lines With a Top Cover," *IEEE Trans. Electromagn. Compat.*, vol. 56, no. 2, pp. 375-384, Apr. 2014.
- [10] D. Deslandes and K. Wu, "Integrated microstrip and rectangular waveguide in planar form," *IEEE Microw. Wireless Compon. Lett.*, vol. 11, no. 2, pp. 68-70, Feb. 2001.
- [11] A. Ali, N. Fonseca, F. Coccetti and H. Aubert, "Novel two-layer broadband 4 × 4 Butler matrix in SIW technology for Ku-band applications," 2008 Asia-Pacific Microwave Conference, 2008, pp. 1-4
- [12] P. Chen et al., "A Multibeam Antenna Based on Substrate Integrated Waveguide Technology for MIMO Wireless Communications," *IEEE Trans. Antennas Propagat.*, vol. 57, no. 6, pp. 1813-1821, June 2009.
- [13] C. Chen and T. Chu, "Design of a 60-GHz Substrate Integrated Waveguide Butler Matrix—A Systematic Approach," *IEEE Trans. Microw. Theory Techn.*, vol. 58, no. 7, pp. 1724-1733, July 2010.
- [14] Q. -L. Yang, Y. -L. Ban, K. Kang, C. -Y. -D. Sim and G. Wu, "SIW Multibeam Array for 5G Mobile Devices," *IEEE Access*, vol. 4, pp. 2788-2796, 2016.
- [15] Q. Sun, Y.-L. Ban, J.-W. Lian, Y. Liu, and Z. Nie, "Millimeter-wave multibeam antenna based on folded C-Type SIW," *IEEE Trans. Antennas Propag.*, vol. 68, no. 5, pp. 3465–3476, May 2020.
- [16] Q. Sun, Y.-L. Ban, Y.-X. Che and Z. Nie, "Coexistence-Mode CRLH SIW Transmission Line and Its Application for Longitudinal Miniaturized Butler Matrix and Multibeam Array Antenna," *IEEE Trans. Antennas Propagat.*, vol. 69, no. 11, pp. 7593-7603, Nov. 2021.
- [17] A. Niembro-Martín et al., "Slow-Wave Substrate Integrated Waveguide," IEEE Trans. Microw. Theory Techn., vol. 62, no. 8, pp. 1625-1633, Aug. 2014.
- [18] H. Jin, K. Wang, J. Guo, S. Ding and K. Wu, "Slow-Wave Effect of Substrate Integrated Waveguide Patterned With Microstrip Polyline," *IEEE Trans. Microw. Theory Techn.*, vol. 64, no. 6, pp. 1717-1726, June 2016.
- [19] H. Jin, Y. Zhou, Y. M. Huang and K. Wu, "Slow-Wave Propagation Properties of Substrate Integrated Waveguide Based on Anisotropic Artificial Material," *IEEE Trans. Antennas Propagat.*, vol. 65, no. 9, pp. 4676-4683, Sept. 2017.
- [20] Y. Zhang et al., "Slow Wave Substrate-Integrated Waveguide With Miniaturized Dimensions and Broadened Bandwidth," *IEEE Trans. Microw. Theory Techn.*, vol. 69, no. 8, pp. 3675-3683, Aug. 2021.
- [21] J. -Y. Deng, Y. -B. Liu, Z. Chen and W. Lin, "Compact Multibeam Antenna Using Miniaturized Slow-Wave Substrate-Integrated Waveguide Rotman Lens for Satellite-Assisted Internet of Vehicles," *IEEE Internet of Things Journal*, vol. 11, no. 4, pp. 6848-6856, Feb.15, 2024.
- [22] H. J. Riblet, "The Short-Slot Hybrid Junction," Proceedings of the IRE, vol. 40, no. 2, pp. 180-184, Feb. 1952.